SAND96-1361C
CONF-960723--3

MONOCHROMATIC IMAGING STUDIES OF SUSTAINED METAL VAPOR ARCS BURNING ON 150 MM DIAMETER MOLTEN IRON ELECTRODES

Rodney L. Williamson and M. Eric Schlienger
Liquid Metal Processing Laboratory
Dept. 1833, M/S 1134
Sandia National Laboratories
P.O. Box 5800
Albuquerque, New Mexico 87185-1134

ABSTRACT

Monochromatic imaging was used to investigate the excited-state density distributions of Fe and Fe^+ in the inter-electrode gap region of a 3,100 A dc metal vapor arc burning between molten iron surfaces in a vacuum arc furnace. Multiple images were acquired at four wavelengths. The images were corrected and Abel inverted to yield the absolute radial intensity distributions for Fe and Fe^+ in the inter-electrode gap region. The results show a structured, axisymmetric plasma consisting of a high density "core" of Fe^+ emitters centered between the electrode surfaces situated against a relatively broad, flat excited-state Fe distribution.

INTRODUCTION

Vacuum arc remelting (VAR) is a process used widely throughout the specialty metals industry in the production of high performance, segregation sensitive and/or air reactive alloys. For example, virtually all titanium and nickel based alloys used to manufacture turbine rotor disks for high performance jet aircraft engines are produced using VAR. Other VAR-processed materials include zirconium for tubing used in nuclear and chemical reactors, various grades of stainless steels used in the manufacture of everything from knife blades to kitchen sinks, and titanium alloys used in many phases of aircraft production as well as increasingly in the manufacture of automobiles, bicycles and sports-related equipment.

The VAR process involves mounting a cylindrical, cast electrode into a cylindrical copper crucible of 0.07-0.15 m larger diameter. Electrode diameters typically range from 0.38 to 0.76 m and lengths from 2.5 to 5.0 m. The crucible is evacuated to a base pressure of ~0.1 Pa and a dc arc is struck between the electrode and some start material on the crucible bottom (called the "stool"). Arc currents range from 5,000 A to 40,000 A depending on the material and sizes being melted. As heat from the arc melts the electrode tip, material drips onto the stool and solidifies. After a period of time, a metal ingot is formed in the crucible. Situated on top of the growing ingot is a pool of molten metal that feeds the solidification process. The electrode is driven down at an average speed that compensates for the shrinking electrode and growing ingot so that the distance between the electrode tip and molten pool, the electrode gap, is held approximately constant throughout the process. This is very important because it affects how the arc energy is distributed in the gap region between the crucible wall and anode pool surfaces.

There are many factors that influence the success of the VAR process. Like electrode gap, many of these factors affect the arc energy distribution. This distribution governs either directly or indirectly the ingot side-wall quality, the electrode tip geometry, the process efficiency, the size and shape of the molten pool, the thermal and electromagnetic driven flows in the pool, and the stability of the solidification interface fed by the pool. Hence, an understanding of how various perturbations adversely affect the VAR process requires an understanding of the basic arc structure in the electrode gap region and how it is affected by the perturbations.

This paper reports efforts to characterize the arc distribution in the electrode gap region of a VAR furnace by using monochromatic imaging to map the atom and ion emission intensities. The study was carried out in a small, specially modified VAR furnace located at the Liquid Metals Processing Laboratory at Sandia National Laboratories. It represents the first of a series of studies aimed at determining how common process disturbances affect the arc distribution between the molten electrode surfaces.

DISTRIBUTION OF THIS DOCUMENT IS UNLIMITED

MASTER

EXPERIMENTAL TECHNIQUES AND PROCEDURES

The experimental furnace is shown in Figure 1. It was modified from the normal VAR configuration so as to have a very short crucible. The crucible diameter is 0.20 m. In a typical experimental trial, a 0.15 m diameter iron electrode was melted at 3,100 A into the crucible until it was full, at which time the arc was imaged through the viewing port. The box at the end of the viewing port contains a fused silica plate that shields the pressure widow (composed of the same material) from arc debris and vapors. The shield window is of much large diameter than the pressure window and may be rotated to allow viewing through clean glass during image acquisition.

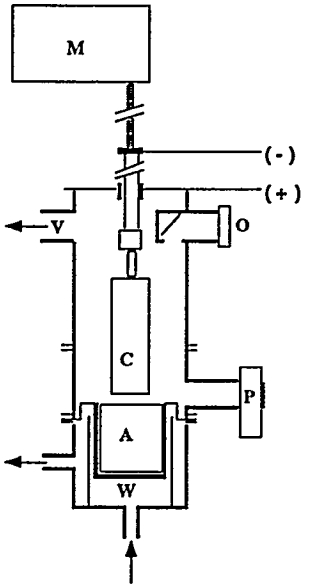

Figure 1. The modified VAR furnace. Key: C -- electrode; A -- anode (ingot); P -- viewing port used for MI; O -- viewing port used for emission spectroscopy; M -- electrode drive motor; V -- vacuum; W -- cooling water.

The monochromatic imaging (MI) system is described in detail elsewhere. [1] It uses a single plano-convex lens (f.l. = 0.200 m) to image the arc through a Czerny-Turner monochromator with a 0.320 m focal length (Instruments SA Mo. HR-320) onto the detector of a CCD camera (Photometrics Mo. CH-250). The input slit of the monochromator was adjusted so as to form a rectangular aperture 7.5×10^{-4} m wide by 1.0×10^{-3} m high. When combined with the 3,600 groove/mm grating used for this study, this aperture yielded a spectral resolution of ~0.8 nm for the instrument. The camera is equipped with a cooled, scientific-grade, 14 bit CCD array. This array is 512 pixels by 512 pixels in size and is coated so as to be UV sensitive. It is interfaced to a Macintosh IIfx computer (Apple, Inc.) using electronics and software supplied by the camera manufacturer. Both the lens and the camera were mounted on translation stages that were independently computer controlled so that, as the monochromator wavelength was changed, the optics were automatically adjusted to keep the image at constant magnification.

The MI system was calibrated using a 40 W deuterium arc lamp that had been calibrated as a UV spectral irradiance standard (Optronics Laboratories, Inc., Mo. UV-40). The system lens was adjusted so that an image of the monochromator output slit was focused onto the CCD array and the input slit was evenly illuminated with the lamp from a distance of 0.30 m. The average number of counts per pixel was determined for the slit image at the wavelengths of interest and adjusted to compensate for the magnification of the imaging system. A calibration constant was then computed for each wavelength in units of μJ/count.

The data presented here were acquired during two experimental melts using a "pure" iron (0.01 ppm C, 0.03 ppm O) electrode. The optical system was adjusted so that the arc center was imaged at one edge of the camera field. Images were acquired at three wavelengths during each melt: two corresponding to either Fe or Fe^+ and one corresponding to a nearby region of the Fe arc spectrum that was dark. The wavelengths investigated, along with their associated transitions, are listed in Table I. [2] Those transitions that are grouped in the table fell within the bandpass of the MI system. Background images were acquired at 366.50 nm and 265.00 nm. Exposure times were set to either 1.00 s or 0.20 s, the shorter time being required to "freeze" the motion of the drips on the electrode tip. The MI system was wavelength calibrated before each melt by imaging a Hg pen lamp at a wavelength near those being used in the experiment. Subsequent to each melt, the acquired images were flat-field corrected, calibrated and Abel inverted to yield the absolute radial intensity distributions at each wavelength. These distributions were then used to calculate the associated excited-state number density distributions for Fe and Fe^+.

A computer program was written to achieve the Abel inversion of the data and the calculation of the excited-state number densities. After the user selects

Arc Species	W.L. (nm)	Transition Identity	A_{ij} (10^8 s^{-1})
FeI	344.39	$a^5D_2 \leftarrow z^5P^\circ_1$	0.073
	344.10	$a^5D_3 \leftarrow z^5P^\circ_2$	0.098
	344.06	$a^5D_4 \leftarrow z^5P^\circ_3$	~0.16
FeI	363.15	$a^5F_3 \leftarrow z^5G^\circ_4$	0.517
FeII	256.25	$a^4D_{7/2} \leftarrow z^4P^\circ_{5/2}$	1.5
	256.35	$a^4D_{5/2} \leftarrow z^4P^\circ_{3/2}$	~0.8
FeII	259.84	$a^6D_{7/2} \leftarrow z^6D^\circ_{5/2}$	1.3
	259.94	$a^6D_{9/2} \leftarrow z^6D^\circ_{9/2}$	2.22

TABLE I The transitions used in this study along with their associated Einstein A-coefficients. Those values marked with a "~" are estimated values from relative intensity information.

the region of the corrected image to be inverted, each line of data across the field of interest is fit using a 5th order polynomial with the linear term set to zero. This is done to ensure that the slope of the fit at the arc center (y = 0) is always zero. After each line of data are fit, the derivative is computed and the Abel integral solved. This integral is given by Equation 1.

$$I(r) = -\frac{1}{\pi}\int_r^R \frac{dI(y)}{dy}\left(y^2 - r^2\right)^{-1/2} dy \qquad (1)$$

The Abel integral is usually solved numerically; however, with the derivative expressed in polynomial form, an explicit solution may be obtained which makes for very fast computation speeds. The program uses the analytical solution to compute the radial intensity distribution for each line in the selected region of the image. The excited-state number density at point r in the plasma is related to the radial intensity distribution function, I(r), by

$$n(r) = \frac{N(r)}{dV} = \frac{N(r)}{Adr} = kI(r) \qquad (2)$$

where k is a constant, N(r) is the number of emitting atoms in the volume element dV located at r, and A is the area of a CCD pixel projected into the plasma volume. The proportionality constant may be found using the following relationship:

$$N = 2\int_0^R kI(r)Adr = kI(y=0) \qquad (3)$$

where N is the total number of emitters in the volume 2AR located at y=0. Given the collection efficiency and transition rate constants, N may be calculated directly from the intensity data. k may then be found and the radial densities calculated.

In addition to the MI data, optical emission spectra were acquired. This was accomplished using viewing port O in Figure 1. The data were acquired using a small monochromator (Instruments SA, Mo. HR-320) equipped with an optical multi-channel analyzer (OMA) detector head (Tracor Northern Mo. TN-6114). A Tracor Northern Mo. TN-6600 controller was used in conjunction with this detector. The controller was interfaced to a computer using electronics and software supplied by the manufacturer. Emission spectral data were used to select sufficiently intense and well isolated lines for the MI studies.

RESULTS AND OBSERVATIONS

Figures 2 through 5 show representative images acquired at the different wavelengths. The intensity data within the rectangular boxes in these images have been Abel inverted. Situated below each image is a surface plot showing the excited-state number density distribution associated with the Abel inverted region. The horizontal axes of these plots are labeled in units of meters and the vertical scales are in units of 10^{13} m^{-3} for the Fe I plots and 10^{12} m^{-3} for the Fe II plots. A contour map is situated below each plot.

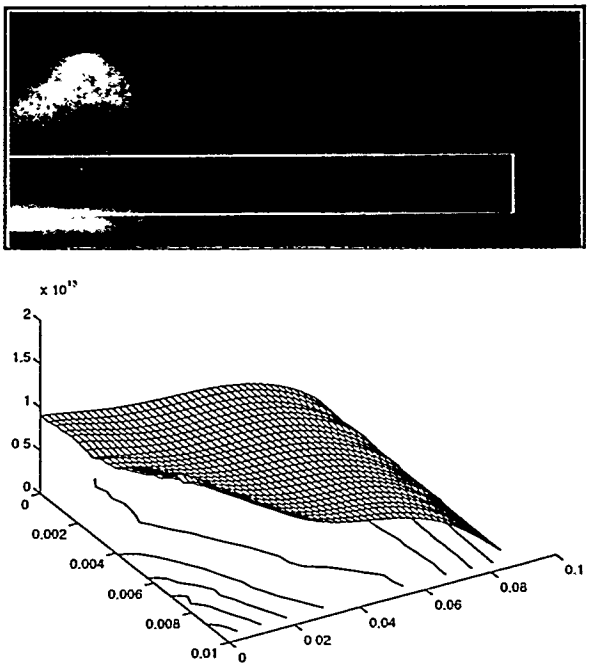

Figure 2. Upper: Monochromatic image acquired at 363.2 nm corresponding to Fe I emission. The region in the box has been Abel inverted. Lower: A surface plot of excited-state number density associated with this region.

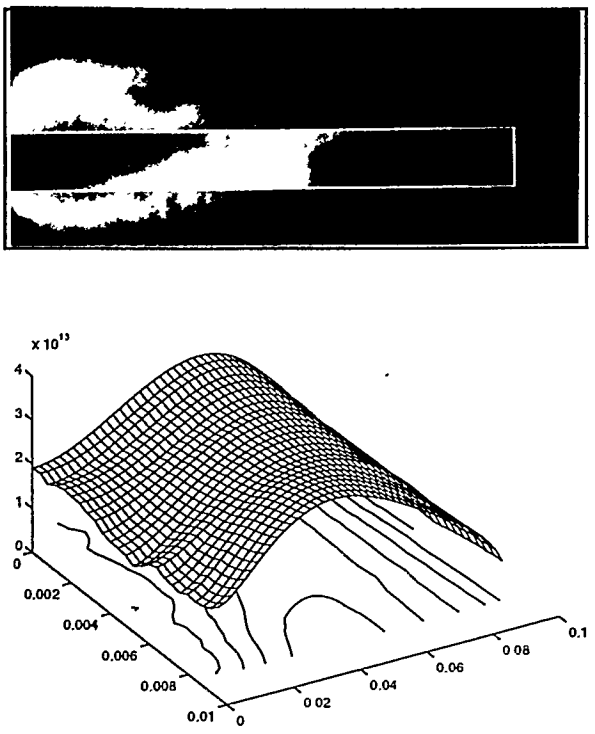

Figure 3. Upper: Monochromatic image acquired at 344.1 nm corresponding to Fe I emission. The region in the box has been Abel inverted. Lower: A surface plot of excited-state number density associated with this region.

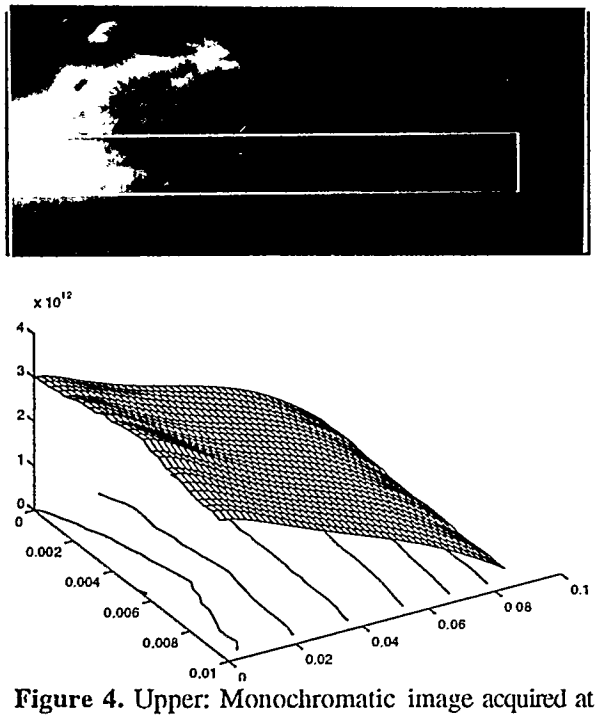

Figure 4. Upper: Monochromatic image acquired at 259.9 nm corresponding to Fe II emission. The region in the box has been Abel inverted. Lower: A surface plot of excited-state number density associated with this region.

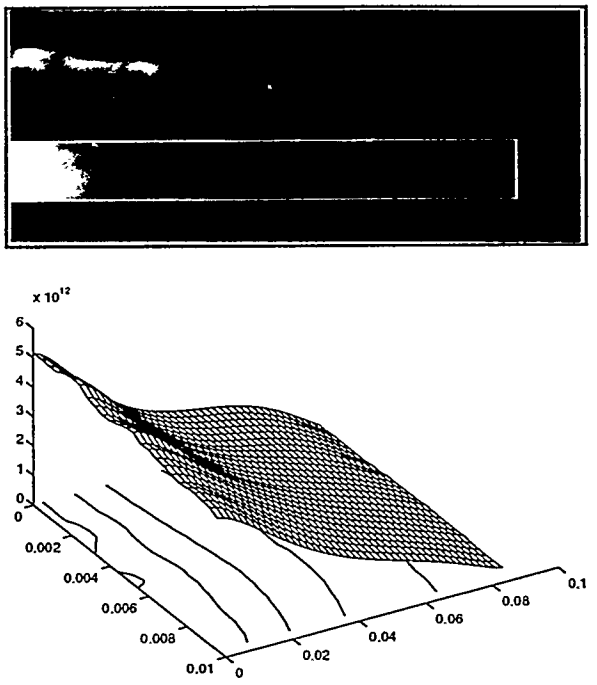

Figure 5. Upper: Monochromatic image acquired at 256.2 nm corresponding to Fe II emission. The region in the box has been Abel inverted. Lower: A surface plot of excited-state number density associated with this region.

It was generally observed that the excited-state atom density is highest near the electrode surfaces and, on average, fills the electrode gap region approximately uniformly (Figure 2). Notice, however, that the distribution at 344.1 nm (Figure 3) shows a local minimum at the arc center. It is believed that this is due to self-absorption. Note also that the excited-state density falls off rapidly in the vicinity of the electrode edge and that the radius of the luminous region decreases near the anode pool. Whereas the atom images simply show unstructured luminosity on the electrode surface, the ion images clearly show cathode spots (Figures 4 and 5). The spot images are not sharp due to the 0.2 s exposure time. It was consistently observed that the excited-state ion density is a maximum at the arc center.

Given the excited-state number densities, it is often possible to calculate the Boltzmann temperatures for the atom and ion distributions in the arc. Indeed, it has been shown that the excited-state number densities in the furnace arc are Boltzmann-like. [3] However, the ability to do this requires that the intensity measurements be made at the designated wavelengths on a time-scale sufficiently short that the arc properties do not change significantly. It was observed in this study that this criterion was not met. By the time the MI system wavelength was scanned

from one emission line to the next, the excited-state density distributions had changed sufficiently that the density ratios were no longer meaningful as a measure of temperature. Hence, no temperature distributions are reported here.

DISCUSSION

The excited-state number densities reported here for Fe and Fe^+ are approximately an order-of-magnitude greater than those obtained in an earlier study of an Alloy 718 arc. [3] This is reasonable because Alloy 718 is only 17.5% Fe by weight and the previous study was carried out at ~30% lower current for the same size electrode. In that study, average number densities were calculated from line-of-sight spectroscopic measurements through the arc center so that radial distributions were not obtained. It was noted then that the number densities characteristic of a VAR furnace arc are significantly smaller that those observed in small-scale laboratory arcs at comparable currents. This was attributed to the fact that, when compared to the cited laboratory studies, the average current density in the furnace arc was ~100 times lower, the volume between the electrodes ~1,000 times larger, and the ambient gas pressure ~100 times higher. The same considerations apply to the results of this study.

The excited-state atom density distribution indicates that significant amounts of material are vaporized at the electrode surfaces forming emissive layers. The cathode layer obscures the cathode spots so that discrete spots are not visible in images acquired at neutral atom wavelengths. As this material diffuses into the electrode gap, it fills the gap to a more-or-less uniform density (Figure 2). Deviations may occur in the immediate vicinity of the pool where the plasma often appears to be anchored to a central area of the anode with a diameter somewhat smaller than that of the cathode. This more luminous region near the pool surface is probably associated with the enhanced plasma density at the arc center described in the Results and Observations and discussed below. The excited-state Fe density distribution derived from the 344.1 nm emission data is suspect and most likely does not accurately reflect the true distribution. Because this wavelength corresponds to a ground-state/excited-state transition, the arc is not perfectly transparent at this wavelength and self-absorption occurs. This, in turn, causes the calculated excited-state density at the arc center to be lower than the actual density.

The Fe^+ data (Figures 4 and 5) clearly indicate that the excited-state ion number density is a maximum at the center of the arc. The induced magnetic field in the arcing region acts to confine conduction electrons near the arc center as well as any positive ions drifting towards the cathode surface. Therefore, it is not surprising that the average excited-state ion density is enhanced in the central region of the arc. This enhanced ion density augments conduction in this region which gives rise to increased heating of the anode pool surface. Hence, it is often observed that a localized hot spot exists in the central region of the pool. Because this is an induced magnetic field effect, as the melting current increases the plasma should become more effectively confined. During high current ($4x10^4$ A) VAR of Ti and Zr alloys, it is observed that the arc is confined completely under the electrode tip and can only be brought out to the edge by applying an external magnetic "stirring" field.

CONCLUSIONS

Radial excited-state number densities were obtained for Fe and Fe^+ in a VAR furnace during melting of pure iron electrodes. The Fe distribution was found to be relatively uniform throughout the electrode gap region, while the Fe^+ distribution had a maximum at the arc center. This causes the anode pool to be more intensely heated near the center relative to the edge. The furnace arc was not sufficiently stable to allow serially acquired images to be used to obtain a temperature distribution. Also, the arc is not optically thin at atomic iron wavelengths corresponding to ground-state/excited-state transitions.

REFERENCES

[1] R. L. Williamson, W. A. Hareland and H. C. Peebles, "Simple Compact Monochromatic Imaging System for Plasma Diagnostics," Appl. Opt. 28 (12), pp. 2201-3 (1988).

[2] J. R. Fuhr, G. A. Martin, W. L. Wiese and S. M. Younger, "Atomic Transition Probabilities for Iron, Cobalt and Nickel," J. Phys. Chem. Ref. Data 10, pp. 305-94 (1981).

[3] R. L. Williamson, F. J. Zanner, L. A. Bertram and H. C. Peebles, "Plasma Studies In Vacuum Arc Remelting," Plasma Processing And Synthesis Of Materials, D. Apelian and J. Szekely, Eds., pp. 365-70 (Materials Research Society, 1987).

ACKNOWLEDGEMENT

This work was performed at Sandia National Laboratories which is supported by the United States Department of Energy under contract DE-AC04-94AL85000. Support for this work was also provided by the Specialty Metals Processing Consortium.

DISCLAIMER

This report was prepared as an account of work sponsored by an agency of the United States Government. Neither the United States Government nor any agency thereof, nor any of their employees, makes any warranty, express or implied, or assumes any legal liability or responsibility for the accuracy, completeness, or usefulness of any information, apparatus, product, or process disclosed, or represents that its use would not infringe privately owned rights. Reference herein to any specific commercial product, process, or service by trade name, trademark, manufacturer, or otherwise does not necessarily constitute or imply its endorsement, recommendation, or favoring by the United States Government or any agency thereof. The views and opinions of authors expressed herein do not necessarily state or reflect those of the United States Government or any agency thereof.